Engineering high-spin state cobalt cations in spinel zinc cobalt oxide for spin channel propagation and active site enhancement in water oxidation

Sun, Yuanmiao; Ren, Xiao; Sun, Shengnan; Liu, Zheng; Xi, Shibo; Xu, Jason Zhichuan

2021

Sun, Y., Ren, X., Sun, S., Liu, Z., Xi, S. & Xu, J. Z. (2021). Engineering high-spin state cobalt cations in spinel zinc cobalt oxide for spin channel propagation and active site enhancement in water oxidation. Angewandte Chemie International Edition, 60(26), 14536-14544. https://dx.doi.org/10.1002/anie.202102452

https://hdl.handle.net/10356/155670

https://doi.org/10.1002/anie.202102452

Engineering High-Spin State Cobalt Cations in Spinel Zinc Cobalt Oxide for Spin Channel Propagation and Active Site Enhancement in Water Oxidation

Yuanmiao Sun[+], Xiao Ren[+], Shengnan Sun*, Zheng Liu, Shibo Xi, and Zhichuan J. Xu*

Abstract: Promoting the initially deficient but cost-effective catalysts to high-performing competitors is of significance in developing better catalysts. Spinel zinc cobalt oxide ($ZnCo_2O_4$) is not considered as a superior catalyst for the electrochemical oxygen evolution reaction (OER), which is the bottleneck reaction in water-electrolysis. Herein, taking advantage of density functional theory (DFT) calculations, we find that the existence of low-spin (LS) state cobalt cations hinders the OER activity of spinel zinc cobalt oxide, as the $t_{2g}^6e_g^0$ configuration gives rise to purely localized electronic structure and exhibits poor binding affinity to the key reaction intermediate. Increasing the spin state of cobalt cations in spinel $ZnCo_2O_4$ is found to propagate a spin channel to promote spin-selected charge transport during OER and generate better active sites for intermediates adsorption. The experiments find increasing the calcination temperature a facile approach to engineer high-spin (HS) state cobalt cations in $ZnCo_2O_4$, while not working for Co_3O_4. The activity of the best spin-state-engineered $ZnCo_2O_4$ outperforms other typical Co-based oxides. Our work pinpoints the critical influence of the spinel composition on the splitting energy of the metals and further on the feasibility of spin state engineering.

The rapid development of industrialization has raised growing concerns toward worldwide energy crisis and environmental problems, such as the shortage of fossil fuels and climate change, which call for a necessary switch of energy resources from traditional fossil fuels to clean and sustainable alternatives. Electrochemical water splitting, which takes advantage of the electric power that can be generated from renewable resources to harvest hydrogen from water, offers an ideal approach to achieve energetic sustainability because of the high energy density and cleanness of hydrogen. However, the slow kinetics and large overpotential required to sustain the counter electrode reaction, the oxygen evolution reaction (OER), greatly hinders the overall efficiency of water electrolysis.[1] Therefore, developing highly active, stable, and low-cost OER electrocatalysts is the decisive objective for realising a clean and sustainable energy infrastructure. To this end, tremendous efforts have been spent on understanding the intrinsic structure-activity relationship of OER on transition metal oxides (TMOs), based on which highly active TMOs composed of earth-abundant elements can be designed with theoretical support. For example, Shao-Horn's group identified that the e_g occupancy of octahedral cations dominates the adsorbate-catalyst interaction and therefore the volcanic activity trend of OER on perovskite oxides.[2a] Based on this theory, perovskite $Ba_{0.5}Sr_{0.5}Co_{0.8}Fe_{0.2}O_{3-\delta}$ (BSCF) with optimal e_g occupancy has been designed and confirmed to be a remarkable OER catalyst. Similarly, the covalency competition in spinel oxides is found crucial in determining the OER activity as it regulates the exposure of active sites.[2b] Based on this, spinel $[Mn]_T[Al_{0.5}Mn_{1.5}]_OO_4$ with a balanced covalency competition was thereafter predicted and identified as an ideal OER catalyst. Years' efforts and accumulations have set up valuable understandings of OER on TMOs, in which the angles from the intermediate-catalyst interaction and the intrinsic structural features of the electrocatalysts have been intensively adapted. However, the perspective from some inconspicuous parts of OER has been long ignored, i.e. the spin configuration of the oxygen product and its coupling with the electrocatalyst, whose role has been recently recognised and emphasized.[3]

A uniqueness of oxygen molecule is that the ground state oxygen favours a triplet spin configuration, i.e. oxygen molecule is paramagnetic. Although this feature has been long identified, its role in determining the efficiency of OER catalysts has been unintentionally neglected. Some pioneer works by J. Gracia et al. have theoretically estimated that TMOs in ferromagnetic (FM) spin ordering generally show more optimal quantum spin exchange interactions (QSEI) and therefore better charge transport ability than those in anti-ferromagnetic (AFM) spin ordering.[3a,4a] In this regard, higher reaction kinetics for triplet oxygen generation can be expected on TMOs with FM spin ordering. This brings out an interesting viewpoint that manipulating the long-range spin ordering in TMOs is an effective way in achieving advanced activity. A following experimental work by Gálan-Mascarós et al. prepared a series of TMOs and observed significant OER enhancement under a moderate magnetic field.[4b] It indicates the generation of triplet oxygen is, to some extent, dependent on the local and long-range spin structures of TMOs. More recently, R. Chen et al. prepared an inversed spinel $LiCoVO_4$ with layered AFM spin structure, within which the high spin state Co^{2+} cations ($t_{2g}^5e_g^2$) can selectively remove spin-oriented electrons from the reactants and facilitate the generation of triplet oxygen, boosting the overall OER kinetics.[4c] Rising evidences have demonstrated that engineering the spin structures is a feasible approach towards enhanced OER activity.[5] However, the potential of this approach is still unclear and, to make full use of it, more mechanistic insights are necessitated to understand the fundamental theoretical basis for the activity enhancement, with which method it can be operatively employed, and to what extent it can enhance the activity of the TMOs that are initially inactive.

In this work, using the OER-deficient $ZnCo_2O_4$ spinel as model catalyst, we report that a spin channel is propagated when engineering high spin state Co^{3+} in $ZnCo_2O_4$ and it is responsible for the greatly enhanced OER activity. The spin engineering can be simply realised by controlling the calcination temperature during synthesis. Spinel $ZnCo_2O_4$ is employed because zinc cations preferentially occupy the tetrahedral sites and fix the cobalt cations in the octahedral sites, which allows an exclusive investigation into the catalytically critical octahedra.[6a] Previous studies have demonstrated the relatively low OER activity of spinel $ZnCo_2O_4$, as Co^{3+} cations in octahedral sites exhibit purely low-spin configuration ($t_{2g}^6e_g^0$) and therefore no unpaired electrons are available to capture and interact with the reactants/intermediates, resulting in poor adsorption.[6] By performing density functional theory (DFT) calculations, we first observed that the octahedra

[*] Dr. Y. Sun, Dr. S. Sun, Dr. X. Ren, Z. Liu, and Prof. Z. J. Xu
School of Materials Science and Engineering, Nanyang Technological University, 50 Nanyang Avenue, Singapore 639798, Singapore, Email: xuzc@ntu.edu.sg (Z. J. Xu)
Dr. S. Sun
Beijing Innovation Center for Engineering Science and Advanced Technology (BIC-ESAT), Beijing Key Laboratory for Magnetoelectric Materials and Devices (BKL-MMD), School of Materials Science and Engineering, College of Engineering, Peking University, Beijing 100871, China, Email: shengnan_sun@pku.edu.cn (S. Sun)
Dr. S. Xi
Institute of Chemical and Engineering Science A*Star, 1 Pesek Road, Singapore 627833, Singapore
Z. Liu and Prof. Z. J. Xu
Nanyang Environment and Water Research Institute (NEWRI), Interdisciplinary Graduate School (IGS), Nanyang Technological University, 1 Cleantech Loop, CleanTech One, Singapore 637141, Singapore.
Prof. Z. J. Xu
Energy Research Institute @ Nanyang Technological University, ERI@N, Interdisciplinary Graduate School, 50 Nanyang Avenue, Singapore 639798, Singapore
Prof. Z. J. Xu
Singapore-HUJ Alliance for Research and Enterprise, NEW-CREATE Phase II, Campus for Research Excellence and Technological Enterprise (CREATE), 138602 Singapore
[+] These authors contributed equally to this work.

units underwent gradual lattice distortion when increasing the spin state of Co cations. This phenomenon was accompanied by the emergence of a spin channel within the $ZnCo_2O_4$ lattice and increased magnetic moment in the adsorbed *OOH species. Therefore, we deduce that raising the spin state will not only promote spin-selected charge transport, but also optimise the orbital interactions between key reaction intermediates and the cation sites, lowering the high free energy gap of the rate-determining step (RDS). Driven by this, a series of spinel $ZnCo_2O_4$ with different fractions of low spin and high spin state Co^{3+} were prepared by controlling the synthesis temperature. Characterizations by X-ray absorption fine structure (XAFS) spectra and Superconducting Quantum Design (SQUID) ruled out the difference in cation valence and pinpointed the gradual increase of high spin state Co^{3+} with the increase of synthesis temperature. Further electrochemical analysis revealed the enhanced OER activity on spin-engineered $ZnCo_2O_4$. The intrinsic activity of the best spin-state-engineered $ZnCo_2O_4$ outperforms other typical Co-based oxides, suggesting the effectiveness of spin engineering. This work highlights the influential factor of spin channel in boosting the OER activity on TMOs, demonstrates the spin structure of Co-based spinels can be straightforwardly engineered, and reflects the strategy of spin engineering is effective even for TMOs with native semiconductor feature.

Spinel $ZnCo_2O_4$ is a normal spinel with Zn^{2+} and Co^{3+} residing in the four-coordinated tetrahedral and six-coordinated octahedral sites, respectively (Figure 1a). The d^{10} electronic configuration of Zn^{2+} makes it catalytically inactive for OER as there are no unpaired electrons available to couple with the reactants or intermediates. Therefore, it has been widely recognised that the Co^{3+} in octahedral units are responsible for the catalytic behaviour of OER on $ZnCo_2O_4$.[6a] Because of the high crystal field splitting energy, Co^{3+} generally favours a low-spin (LS) state ($t_{2g}^6e_g^0$) in octahedral environment[7], where the t_{2g} orbitals are fully occupied and e_g orbitals fully empty (Figure 1b). This gives rise to a purely localized electronic structure and therefore an intrinsic semiconductor feature.[6a,8] As a result, spinel $ZnCo_2O_4$ is not considered as a highly active catalyst for OER.[6b,9] Nevertheless, the empty e_g orbitals offers an opportunity to engineer the LS state Co^{3+} into high spin state, which, from an electronic point of view, will significantly change the catalytic nature of $ZnCo_2O_4$. As illustrated in Figure 1b, the empty e_g orbitals can allow up to two unpaired electrons to reside in, forming the intermediate-spin (IS) state ($t_{2g}^5e_g^1$) and high-spin (HS) state ($t_{2g}^4e_g^2$), respectively. The gradual occupation of e_g orbitals induces the emergence of a spin density around Co^{3+} cations, which further brings about a spin hole in oxygen through exchange interactions.[3a,4a,10] Consequently, electrons become delocalized and a spin channel connecting the cobalt cations and oxygen anions will generate, creating an unblocked spin pathway to facilitate charge transport during electrocatalysis.

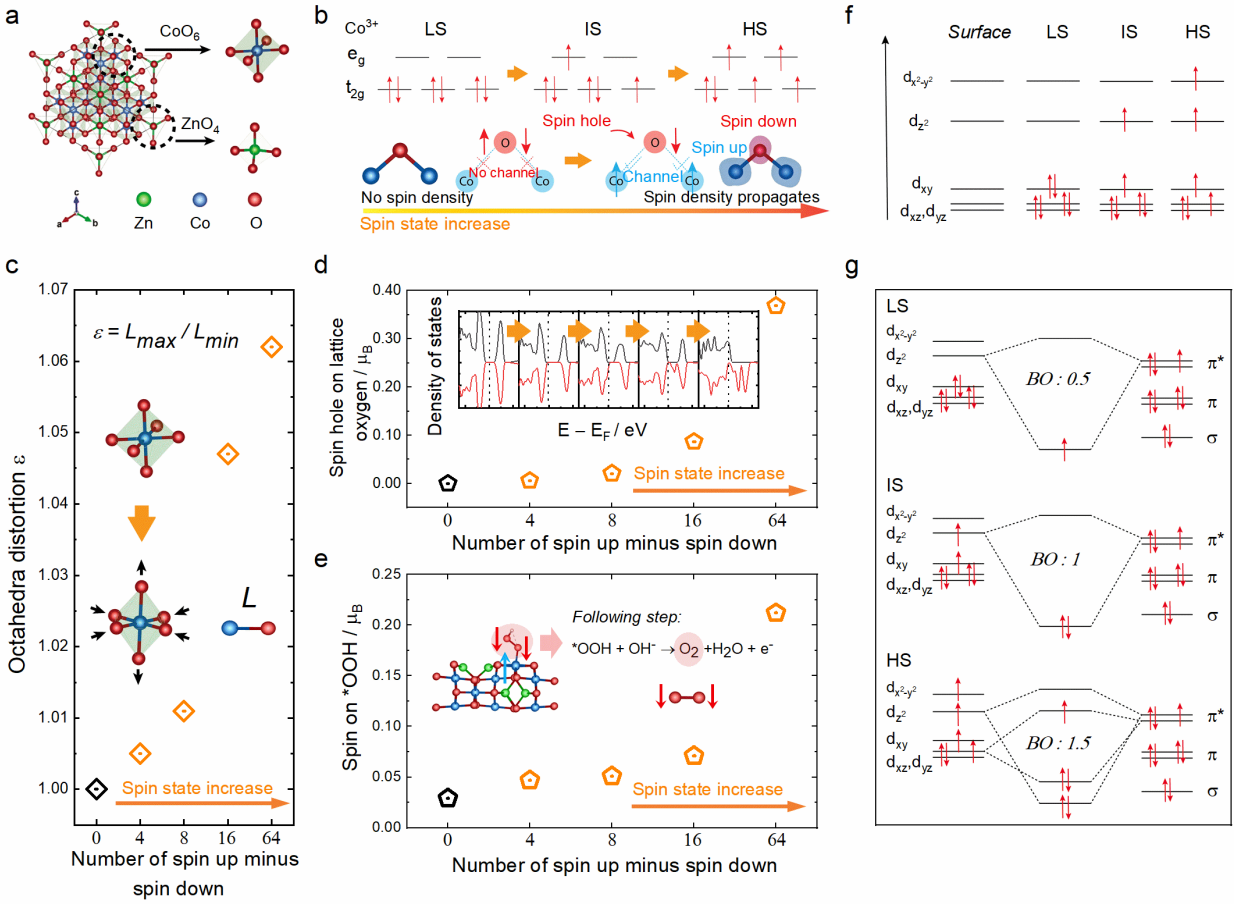

Figure 1. a) Crystal structure of spinel $ZnCo_2O_4$ with Zn and Co staying in the tetrahedral and octahedral sites, respectively. b) Illustration of the evolution of Co^{3+} spin state and Co–O–Co spin channel during the process of raising the cobalt spin state. c) The octahedra distortion (ε) during spin state increase. d) The calculated bulk oxygen magnetization (μ_B) of $ZnCo_2O_4$ during spin state increase. The inserted patterns show the density of states (DOS) of $ZnCo_2O_4$ during spin state increase. The dashed lines in DOS show the Fermi level. e) The average magnetization (μ_B) on oxygen atoms of the adsorbed *OOH species. Here the *OOH was adsorbed on the (110) surface of spinel $ZnCo_2O_4$. The methods of increasing the spin state of cobalt cations are summarized in supplementary information. f) *d*-electron configurations of cobalt cation in different spin state at the surface. g) The orbital interactions between cobalt cations in different spin state and the *OOH intermediate. The bond order (BO) is also shown in the figure. The BO is defined as half the difference between the number of bonding electrons and the number of antibonding electrons (bond order = (number of bonding electrons – number of antibonding electrons) / 2).

To verify this, density functional theory (DFT) calculations were first performed to study the electronic structure of spinel $ZnCo_2O_4$ with controlled spin state of cobalt cations (more details are summarized in Supplementary Information). As shown in Figure 1c, when manually increasing the unpaired spins in $ZnCo_2O_4$, an apparent phenomenon is that the octahedral units undergo a lattice distortion, where the more the unpaired spins are, the more severe the lattice distortion is. This is because the increase of cobalt spin state forces the two originally empty e_g orbitals to be steadily occupied, which gives rise to a degenerate electronic ground state. This electronic state is unstable and induces Jahn-Teller effect to lower the energy as well as symmetry of the system.[11] As a result, the degeneracy is broken and the octahedral units exhibit elongated distortion. Another pivotal change in the electronic structure is the emergence of spin hole in lattice oxygen. The spin hole of lattice oxygen reflects the magnitude of spin density on oxygen, thereby can be used as a quantitative index of the spin channel between cobalt cations and oxygen anions. As displayed in Figure 1d, the magnetization of lattice oxygen in $ZnCo_2O_4$ is 0 μ_B, suggesting non-existence of spin hole and therefore no spin channel lies in between cobalt cations and oxygen anions. When manually increasing the spin state of cobalt cations, the magnetization of lattice oxygen steadily and powerfully rises, implying the emergence and intensification of the spin channel. The inserted density of states (DOS) patterns in Figure 1d provide a more visual illustration of the spin channel evolution during the process of cobalt spin state increase. For $ZnCo_2O_4$ with no spin manipulation, the spin-up and spin-down densities are completely symmetric and no channel lies across the Fermi level. When the spin state of Co^{3+} is manually raised, the symmetry of DOS is gradually destroyed. Meanwhile, the electronic density starts to become continuous as a result of the delocalized electrons and eventually, a channel connecting the states below and across the Fermi level appears and propagates. Note that the channel is strictly propagated in the spin-up domain, suggesting spin-selected charge transport is induced and promoted.[3b] Besides the aspect of charge transport, we also evaluated the thermodynamic characteristics of $ZnCo_2O_4$ with HS state Co^{3+}. According to previous study[12], the RDS of OER on LS state $ZnCo_2O_4$ is the coupling between OH^- and *O to form *OOH (*O + OH^- →*OOH + e^-, * denotes the active site). This step forms the O–O bond, the spin magnitude on which is crucial in determining the overall efficiency of the triplet oxygen generation. Since LS state Co^{3+} does not possess unpaired spin, the coupling between adsorbed oxygen atom and OH^- produces little magnetization on the formed *OOH (0.029 μ_B per oxygen atom, Figure 1e). By steadily increasing the spin state, the magnetization on *OOH increases because of two reasons. On one hand, the increased spin on Co^{3+} makes the originally empty e_g orbitals partially occupied, which forms stronger ligand bond with oxygen-related species compared to the case of purely empty orbitals.[2a] This helps stabilize Co–O–O bond and generate spin pathway in between Co–O–O. On the other hand, the delocalized electrons originated from high spin state Co^{3+} have higher chances to hop into oxygen orbitals, thereby increasing the spin density on oxygen. The bond strength between cobalt cations and the *OOH intermediate can be analysed through plotting the spin-orbital interaction diagrams. Figure 1f displays the spin configurations of Co^{3+} at the surface, where reaction takes place. Due to symmetry conservation, the interactions between the d_{x2-y2} and d_{xy} orbitals of Co^{3+} cation and the orbitals of OER intermediates are negligible.[3b,13] Therefore, only the orbitals of d_{z2}, d_{yz}, and d_{xz} are shown in the diagrams (Figure 1g). Because of the empty e_g orbitals, LS state Co^{3+} shows weak interaction with *OOH intermediate, where the bond order (BO) is only 0.5. With the increase of Co^{3+} spin state, more unpaired spins are available to couple with the p orbitals of *OOH. As a result, more bonding electrons are formed and the bond order of Co-*OOH continues to increase. Since a higher value of BO indicates a stronger binding configuration, it can be expected that the *OOH intermediate can be practically stabilized on HS state Co^{3+}. Subsequent DFT calculations of the reaction pathway reveal the strengthened adsorption of *OOH intermediate and a consecutive free energy decrease of RDS (Figure S1), suggesting an enhanced thermodynamic feature of $ZnCo_2O_4$ with HS state Co^{3+}. Therefore, the DFT calculations have evidenced that engineering HS state Co^{3+} in $ZnCo_2O_4$ will not only create unblocked spin channel to boost spin-selected electron transport, but also facilitate the overall thermodynamic property for OER.

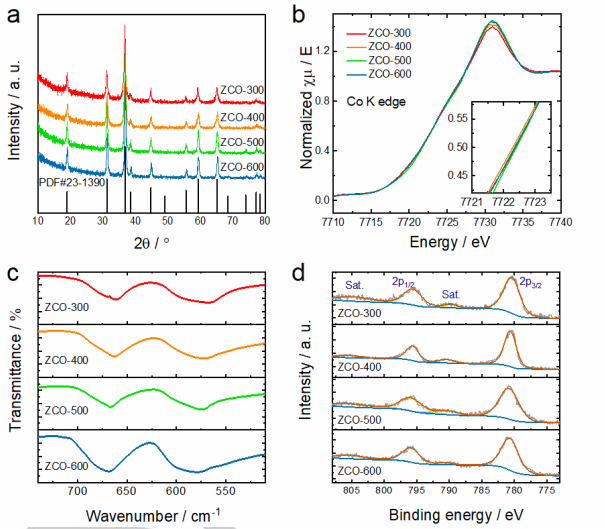

Figure 2. a) XRD patterns of the as-prepared spinel $ZnCo_2O_4$ samples and the standard pattern PDF#23-1390. b) XANES spectra of Co-K edge. The inserted pattern magnifies the spectra in between the range from 2231 eV to 7723 eV. c) FT-IR spectra of the as-prepared spinel $ZnCo_2O_4$ samples. d) The Co 2p XPS spectra of the as-prepared spinel $ZnCo_2O_4$ samples.

Motivated by the DFT predictions, a series of $ZnCo_2O_4$ with different spin state of Co^{3+} were prepared. The samples were synthesized by a nitrate decomposition method followed by different heat treatment temperatures (see details in Supplementary Information). Specifically, four samples respectively calcinated at 300, 400, 500, and 600 °C were prepared (denoted as ZCO-300, ZCO-400, ZCO-500, and ZCO-600, respectively). The crystal structures of the as-synthesized $ZnCo_2O_4$ samples were confirmed by X-ray diffraction (XRD) analysis. As displayed in Figure 2a, the diffraction peaks of the four samples fit well with that of the standard $ZnCo_2O_4$ (PDF#23-1390), suggesting a typical cubic spinel structure with Fd3m space group. The X-ray fluorescence (XRF, Figure S2) and inductively coupled plasma optical emission spectrometry (ICP-OES, Table S1) results indicate all the as-prepared samples remain stoichiometric $ZnCo_2O_4$. The occupancy and valence state of the cobalt cations were probed by X-ray absorption fine structure (XAFS) technique. Figure 2b shows the X-ray absorption near-edge spectroscopy (XANES) spectra of cobalt K-edge, in which no peak arises in the pre-peak region, demonstrating no tetrahedral cobalt exists and thereby all the cobalt cations should reside in octahedral sites. Similarly, the zinc K-edge spectra (Figure S3) indicates all the zinc cations are tetrahedrally coordinated. Therefore, it can be deduced that the as-prepared $ZnCo_2O_4$ samples all exhibit normal spinel structure, where Zn and Co occupy the tetrahedral and octahedral sites, respectively. Besides, the peak positions and shapes of the cobalt K-edge spectra of the four samples are close to each other, suggesting the valence states of cobalt cations are similar. The inserted pattern in Figure 2b magnifies the spectra in between the energy range from 7721 eV to 7723 eV, which gives a more evident illustration of the nearly unchanged valence state of cobalt cations. Further spectral fitting of the extended X-ray absorption fine structure (EXAFS) (Figure S4) confirms the changed M–O bond lengths, indicative of the emergence of lattice distortion. The Fourier Transform Infrared (FTIR) spectroscopy technique was then employed to probe the local chemical bond change of the samples (Figure 2c). The bands at around 570 cm^{-1} and 665 cm^{-1} correspond to vibrations of the Co-O and Zn-O stretching, respectively.[14a] With the increase of calcination temperature, two obvious phenomena begin to occur. First, the peak shape becomes broader, which suggests a steady decrease of homogeneousness of M-O bond.[14b] Secondly, the vibration peaks are observed to shift to higher wavenumber direction, indicative of higher M-O vibration energy resulted from

changed Co-O bond length.[14c] Both observations signify the change in chemical bond and therefore the emergence of lattice distortion. Further analysis of the metal oxidation states and adsorbed species were performed utilizing X-ray photoelectron spectroscopy (XPS) technique (Figure 2d and Figure S5). The XPS general spectrum in Figure S5a gives a further indication of the presence of zinc, cobalt, and oxygen. The peaks centred at around 530 eV and 531.8 eV in O 1s spectrum (Figure S5b) correspond to O^{2-} (lattice oxygen) and surface adsorbed OH^-, respectively.[15a] It is observed that the O^{2-} peaks of the four samples slightly shift to higher binding energy level with the increase of calcination temperature. This may be caused by the increased powder size which reduces the specific surface area at higher temperature.[15b] The decreased specific surface area is evidenced by Brunauer–Emmett–Teller (BET) analysis, which is shown in Figure S6. The Co 2p spectrum (Figure 2d) presents prominent peaks at around 781.2 eV and 796.3 eV (detailed peak values of the four spectra are summarized in Table S2), which can be ascribed to Co $2p_{3/2}$ and Co $2p_{1/2}$ of Co^{3+}, respectively. The spin-orbital splitting of the two peaks is ~15 eV, consistent with the data reported in previous studies.[15a,c] The oxidation state of cobalt cations can also be estimated using the information of the satellite peaks. As demonstrated by previous studies[15d,e], another possible and effective principle for evaluating the cobalt valence state is the energy gap between the Co main peak and the satellite peak, in which an energy gap of ~ 6 eV indicates a +2 valence state while a value around 9~10 eV is associated with a +3 valence state. As shown in Figure 2d, the satellite peaks are detected at ~790.5 eV and ~805.7 eV, giving rise to a gap of ~9.3 eV and ~9.4 eV from the Co $2p_{3/2}$ and Co $2p_{1/2}$ peak, respectively. This additionally evidences the cobalt oxidation state in all the samples are +3. As demonstrated in previous study[6a], the charge on octahedral cobalt is an influential factor that can alter the OER activity on Co-containing spinel oxides; in this work, the consistency of cobalt oxidation state guarantees an exclusive investigation into the spin-dependent OER activity on spinel $ZnCo_2O_4$.

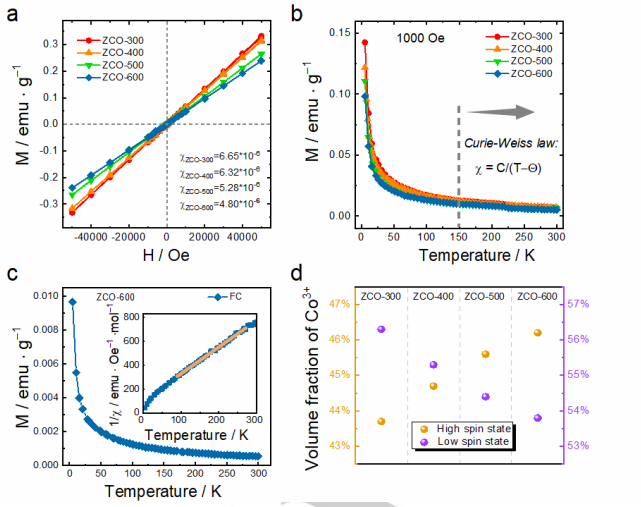

Figure 3. a) Hysteresis loops of the as-prepared spinel $ZnCo_2O_4$ samples recorded at room temperature (300 K). b) Temperature-dependent magnetization characterizations of the as-prepared samples at H=1000 Oe. The characterizations were performed under field-cooling procedures in between a temperature range from 5 to 300 K. c) The temperature-dependent magnetization curve of ZCO-600. The inserted pattern shows the fitted susceptibility versus. temperature based on Curie-Weiss law. d) The calculated volume fraction of HS and LS state Co^{3+} in the four samples.

The magnetic properties and their related spin information were thereafter characterised by Superconducting Quantum Design (SQUID) technique. Taking advantage of superconducting loops containing Josephson junctions, this approach allows the detection of extremely subtle magnetic field. Figure 3a shows the recorded magnetization curves in magnetic field from -50 to 50 kOe. The magnetization curves of all the samples show similar profile and no hysteresis feature shows up, suggesting paramagnetic behaviors under ambient conditions.[16] The changed magnetic susceptibility of the four samples confirms the changed spin structures. Further temperature-dependent magnetization characterizations were carried out under field-cooling procedures at H=1000 Oe in between a range from 5 to 300 K (Figure 3b). In high temperature domain (above 150 K), the susceptibilities derived from the magnetizations ($\chi = M/H$) obey a paramagnetic Curie-Weiss law: $\chi = C/(T - \Theta)$, where C and Θ stand for the Curie constant and Curie-Weiss temperature, respectively.[17] The fitting result (susceptibility versus. T) for ZCO-600 is shown in the inserted pattern of Figure 3c, while those of the other samples are summarized in Figure S7. Based on the fitting results, the effective magnetic moment μ_{eff} can be acquired through $\mu_{eff} = \sqrt{8C}\ \mu_B$ (more details are provided in Table S3). For octahedrally coordinated Co^{3+}, controversies exist in decades to conclude whether the higher spin state of Co^{3+} in room temperature is an intermediate-spin state ($t_{2g}^5e_g^1$) or a mixture of LS state ($t_{2g}^6e_g^0$) and HS state ($t_{2g}^4e_g^2$).[18] However, most of the recent experimental and theoretical studies highlight that the mixture of LS and HS states is more reasonable.[14c,17,19] Therefore, we treated the spin state of Co^{3+} as a mixture of HS state (4.9 μ_B) and LS state (0 μ_B) in this work. Using these values, the volume fractions of Co^{3+} in HS and LS states can be obtained by the following equation:

$$\mu_{eff} = g\mu_B\sqrt{S_{LS}(S_{LS}+1)V_{LS} + S_{HS}(S_{HS}+1)V_{HS}}$$

where S_{LS} (= 0) and S_{HS} (= 2) are the number of unpaired spins in e_g orbitals for LS and HS state Co^{3+}, respectively; V_{LS} and V_{HS} (= 1 – V_{LS}) are the volume fractions for Co^{3+} in LS and HS states, respectively; g is the Landé g-factor and equals to 2 for electrons. The calculated volume fractions of Co^{3+} in LS and HS states are exhibited in Figure 3d and more details of the calculation procedures are listed in Table S3. As shown in Figure 3d, with the increase of calcination temperature, the fraction of HS Co^{3+} steadily increases, suggesting more LS Co^{3+} have been engineered into HS state. Besides, the Co 3s XPS spectra can also be used as an indicator of the cation spin state in TMOs. The exchange interactions between unpaired 3d electrons and 3s hole electrons can split the 3s core into two peaks.[20] The magnitude of the splitting is proportional to (2S + 1), where S is the local 3d spin. As displayed in Figure S8 and Table S4, the increased Co 3s core splitting further confirms the increased cobalt spin state with the increase of calcination temperature. Therefore, it is persuasively demonstrated that controlling the calcination temperature is an effective strategy to engineer HS state Co^{3+} in spinel $ZnCo_2O_4$.

After pinpointing the increase of HS state Co^{3+} in $ZnCo_2O_4$, electrochemical OER analysis of the four samples were performed. The OER performances of the as-prepared samples were recorded in O_2-saturated 1 M KOH. To probe into the intrinsic OER activity of the samples, current densities were normalized by the catalysts' surface area rather than the electrode geometric area.[21] The surface area of the $ZnCo_2O_4$ spinels were quantified by BET technique (Figure S6), which has been proved to be suitable for measuring the surface area of metal oxides in powder form.[21] Figure 4a presents the CV curves in between the range from 1.52 V to 1.62 V (vs. RHE). As obviously presented, ZCO-600 exhibits the best OER activity among the four samples while ZCO-300 the worst, demonstrating the effectiveness of engineering HS Co^{3+} for improved OER activity. The electrochemical impedance spectra (EIS) of the samples (Figure 4b) confirms the enhanced ion transport at the electrode-electrolyte interface on spin-engineered $ZnCo_2O_4$ samples. The TEM patterns of ZCO-600 before and after OER (Figure S9) indicate no surface reconstruction occurred and the structure remained a spinel frame. The OER activity *vs.* HS Co^{3+} fraction in the four $ZnCo_2O_4$ samples (Figure 4c) highlights the strong correlation between the HS Co^{3+} and the enhanced reaction activity. In ZCO-300 where HS Co^{3+} fraction is relatively small (43.7%), a high potential of ~1.62 V is required to achieve a current density of 25 μA cm^{-2}. The potential decreases to ~1.58 V in ZCO-600 where HS Co^{3+} fraction is increased to 46.2%. This signifies the huge potential of utilizing the approach of spin engineering in achieving remarkable OER activity on transition metal oxides as slight spin state change is sufficient to induce a remarkable activity enhancement. The comparison between the intrinsic activity of spin-engineered $ZnCo_2O_4$ and that of the other typical Co-based oxides was then performed. As shown in Figure 4d, steadily engineering HS state Co^{3+} observably raises the

turnover frequency (TOF) of the originally OER-inactive $ZnCo_2O_4$. Moreover, the intrinsic activity of ZCO-600 is even higher than that of CoO_xH_y[22] and Co_3O_4[6a] (Figure 4e), suggesting the decent activity of spin-engineered $ZnCo_2O_4$. However, it is worth noting that we did not observe the similar remarkable activity difference among the Co_3O_4 annealed in the same temperature range (from 300 °C to 600 °C), which brings about an interesting discussion about the applicability of this strategy in engineering the spin state of cations in TMOs (Figure 4g). Generally, for the catalytically active octahedral units, the transition from LS state to IS and HS state involves the migration of electrons from the low-lying t_{2g} orbitals to the high-lying e_g orbitals, during which an energy gap (the splitting energy between t_{2g} and e_g orbitals) needs to be surmounted (Figure 4f). Because octahedrally coordinated Co^{3+} commonly exhibits higher crystal splitting energy than spin pairing energy[23], in most cases, the d^6 Co^{3+} cation favours a LS state configuration. However, the exact splitting energy of Co^{3+} in a coordination complex varies by the influence of the surrounding ligands. Therefore, for a given temperature, the possibility of HS state Co^{3+} formation largely depends on the splitting energy between t_{2g} and e_g orbitals. In spinel frame where a M_T–O–M_O (M_T and M_O represent the metal cations in tetrahedral and octahedral sites, respectively) backbone spreads along the lattice, the type of tetrahedral cation plays nonnegligible role in shaping the electronic structure of the oxygen ligand and, consequently, the octahedral cation.[6a] As shown in Figure 4h, the calculated splitting energy of the octahedrally coordinated LS Co^{3+} for spinel $ZnCo_2O_4$ and Co_3O_4 is 1.13 eV and 1.35 eV, respectively. The lower splitting energy of $ZnCo_2O_4$ enables a higher possibility of spin state transition towards HS Co^{3+}. Besides, compared to Co_3O_4, the lower splitting energy of $ZnCo_2O_4$ might be possible for more sensitive spin-crossover-related applications, where a transition in spin state is necessary and crucial. Thus, to take the advantage of this simple strategy for engineering the spin state of cations in spinel TMOs, tuning the composition and the cation occupation towards a low splitting energy might be the prerequisite. It should be noted that the cobalt with oxygen ligands in oxides usually gives the multiplicity of spin state. Thus, for cobalt-based spinel oxides, a possible way to enable the spin state change by the simple approach reported here is tuning the type of tetrahedral cation. It shapes the electronic structure of the oxygen ligand and octahedral cation through the M_T–O–M_O backbone and therefore may influence the splitting energy of the octahedrally coordinated cobalt cations. However, for other commonly employed 3d transition metals, such as Mn, Fe, and Ni, the situations are slightly different and need to be case-by-case analysed. For manganese cations, the spin state is usually in HS state because of the smaller crystal field splitting energy than spin-pairing energy in octahedral environment.[24] Therefore, tuning its spin state may not be feasible in manganese-based spinel oxides. For iron cations, the d^5 spin configuration generally favours a HS state due to the Hund's rules, which means spin engineering might be inconspicuous. However, it's worth to note that in some inverse spinels, i.e. Fe_3O_4, the octahedral sites can be occupied by both Fe^{2+} and Fe^{3+} cations. In this case, tuning the spin state of Fe^{2+} is possible. For nickel cations, both LS ($t_{2g}^6e_g^1$) and HS ($t_{2g}^5e_g^2$) state could possibly exist within the d^7 spin configuration, indicating the possibility of the spin state tuning. The stability test of ZCO-600 was carried out by repeating CV scan for 500 cycles and the chronoamperometry method at 1.63 V (*vs.* RHE) for more than 8 hrs. As displayed in Figure 4i, the electrochemical performance of ZCO-600 remains almost unchanged within 200th test period and only trivial amounts of current density have dropped during the 300th to 500th cycle, demonstrating its excellent stability. A more straightforward illustration in Figure 4j further reveals the limited drop in 30000 s.

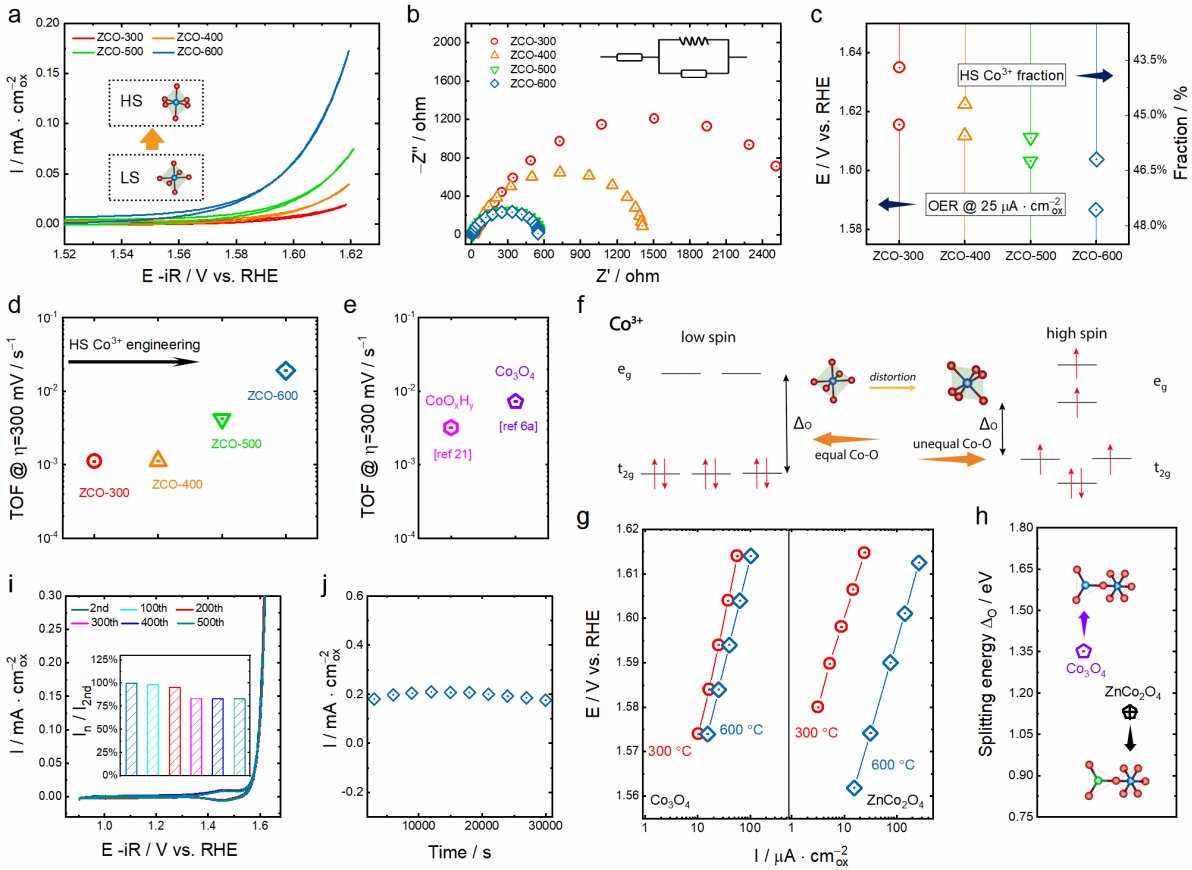

Figure 4. a) The CV curves of the as-prepared $ZnCo_2O_4$ samples. b) The electrochemical impedance spectra (EIS) of the samples. c) The HS Co^{3+} fraction vs. the potential at 25 μA cm_{ox}^{-2} of the as-prepared $ZnCo_2O_4$ samples. d) The calculated turnover frequency (TOF) of the four as-prepared samples. e) The TOF of CoO_xH_y and Co_3O_4 from reference papers. f) Illustration of the crystal splitting energy (Δ_O) of octahedrally coordinated cobalt cations in LS state and HS state. g) Tafel plots of $ZnCo_2O_4$ and Co_3O_4. The data of Co_3O_4 are taken from ref. 20a. h) The calculated crystal splitting energy of octahedrally coordinated LS state cobalt in spinel $ZnCo_2O_4$ and Co_3O_4. i) The stability test of ZCO-600 with 500 CV cycles. The inserted pattern shows the fraction of the current density (at 1.5 V vs. RHE) in reference to the 2nd cycle. j) The chronoamperometry stability test (@ 1.63 V vs. RHE) of ZCO-600 for 30000 s.

The pivotal feature behind the phenomenon is that LS state Co^{3+} has purely empty e_g orbitals and all spins are paired up in t_{2g} orbitals (Figure 5). This creates strictly localized electronic structure, resulting in completely symmetric electron density. Consequently, no spin channel lies across the Fermi level and spin-selected charge transport cannot be promoted. Besides, the $t_{2g}^6e_g^0$ spin configuration makes the orbital coupling between surface Co–O and OH^- difficult. As a result, the key *OOH intermediate adsorbs weakly at the Co site, requiring a high potential to neutralize the RDS of the hydro-oxidization of *O. Therefore, neither the spin-selected charge transport nor the proper intermediate adsorption can be expected on LS Co^{3+}. The transformation from LS state to HS state enables spin occupancy in e_g orbitals, which gives rise to a distorted CoO_6 octahedra and delocalized electronic structure. Two subsequent features are then induced. On one hand, the delocalized electron density propagates a spin channel across the Fermi level (Figure 5), promoting the spin-selected charge transport during OER. On the other hand, the (partially) occupied e_g orbitals form stronger chemical bond with the key *OOH intermediate, which significantly lowers the potential to counterbalance the RDS. Thus, engineering HS state Co^{3+} in spinel zinc cobalt oxide not only propagates a spin channel for promoted spin-selected charge transport, but also improves catalytic sites for enhanced orbital interactions.

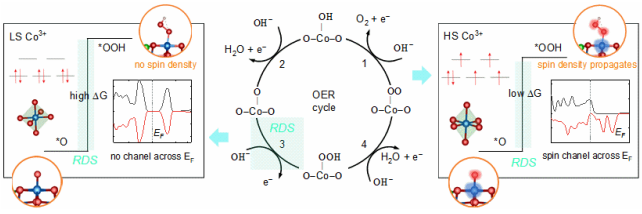

Figure 5. A schematic illustration of OER catalysed by LS Co^{3+} and HS Co^{3+} in spinel $ZnCo_2O_4$.

In summary, employing spinel $ZnCo_2O_4$ as model catalyst, we have elaborately demonstrated the effectiveness of spin engineering for enhanced OER electrocatalysis. The DFT calculations identify the emergence and propagation of a spin channel from the initially insulating $ZnCo_2O_4$ during spin engineering. The spin-engineered $ZnCo_2O_4$ is predicted to possess both spin-selected charge transport and stabilized *OOH intermediate. Subsequent experiments establish a simple and straightforward approach to engineer high spin state Co^{3+} in $ZnCo_2O_4$ by controlling the calcination temperature. The best-performing ZCO-600 oxide with large amounts of high spin state Co^{3+} exhibits decent OER activity that outperforms other Co-based oxides and can durably last under operating conditions. Our work emphasizes the rationality and benefits of engineering the spintronic structure of metal oxides for advanced electrocatalysis. Further explorations on wider varieties of transition-metal oxides may bring about more mechanistic understandings of spin-catalysed reactions and promote oxygen electrocatalysis to a new level where the magnetic properties of catalyst can be precisely manipulated to achieve optimal reaction performance.

Acknowledgment

Dr. S. Sun thanks the funding support from Beijing Natural Science Foundation Program 2212029 and National Natural Science Foundation of China-Youth Science Fund (Grant No. 52001009). All authors thank the Facility for Analysis, Characterisation, Testing and Simulation (FACTS) at the Nanyang Technological University for materials characterizations. This work was supported by Singapore Ministry of Education Tier 2 Grant (MOE2018-T2-2-027), the National Research Foundation, Prime Minister's Office, Singapore under its Campus for Research Excellence and Technological Enterprise (CREATE) programme.

Key words: high-spin cobalt cation • spinel oxide • spin channel • active site • water oxidation

Reference

[1] a) Y. Guo, Y. Tong, P. Chen, K. Xu, J. Zhao, Y. Lin, W. Chu, Z. Peng, C. Wu, Y. Xie, *Adv. Mater* **2015**, *27*, 5989-5994; b) D. A. Kuznetsov, B. Han, Y. Yu, R. R. Rao, J. Hwang, Y. Román-Leshkov, Y. Shao-Horn *Joule* **2018**, *2*, 225-244; c) Z. J. Xu, *Nano-Micro Lett.* **2018**, *10*, 8; d) X. Zhao, H. Zhang, Y. Yan, J. Cao, X. Li, S. Zhou, Z. Peng, J. Zeng, *Angew. Chem. Int. Ed.* **2017**, *56*, 328-332; *Angew. Chem.* **2017**, *129*, 334-338.

[2] a) J. Suntivich, K. J. May, H. A. Gasteiger, J. B. Goodenough, Y. Shao-Horn, *Science* **2011**, *334*, 1383-1385; b) Y. Sun, H. Liao, J. Wang, B. Chen, S. Sun, S. Ong, S. Xi, C. Diao, Y. Du, J. Wang, M. B. Breese, S. Li, H. Zhang, Z. J. Xu, *Nature Catal.* **2020**, *3*, 554-563.

[3] a) J. Gracia, *Phys. Chem. Chem. Phys.* **2017**, *19*, 20451-20456; b) Y. Sun, S. Sun, H. Yang, S. Xi, J. Gracia, Z. J. Xu, *Adv. Mater.* **2020**, *32*, 2003297; c) J. Zhang, Y. Yan, B. Mei, R. Qi, T. He, Z. Wang, W. Fang, S. Zaman, Y. Su, S. Ding, B. Xia, *Energy Environ. Sci.* **2021**, *14*, 365-373; d) J. Qian, T. Wang, Z. Zhang, Y. Liu, J. Li, D. Gao, *Nano Energy* **2020**, *74*, 104948.

[4] a) J. Gracia, R. Sharpe, J. Munarriz, *J. Catal.* **2018**, *361*, 331-338; b) F. A. Garcés-Pineda, M. Blasco-Ahicart, D. Nieto-Castro, N. López, J. R. Gálan-Mascarós, *Nature Energy* **2019**, *4*, 519-525; c) R. Chen, Y. Sun, S. Ong, S. Xi, Y. Du, C. Liu, O. Lev, Z. J. Xu, *Adv. Mater.* **2020**, *32*, 1907976.

[5] a) Y. Tong, Y. Guo, P. Chen, H. Liu, M. Zhang, L. Zhang, W. Yan, W. Chu, C. Wu, Y. Xie, *Chem* **2017**, *3*, 812-821; b) G. Shen, R. Zhang, L. Pan, F. Hou, Y. Zhao, Z. Shen, W. Mi, C. Shi, Q. Wang, X. Zhang, J. Zou, *Angew. Chem. Int. Ed.* **2020**, *59*, 2313-2317; *Angew. Chem.* **2020**, *132*, 2333-2337; c) Y. Liu, C. Xiao, M. Lyu, Y. Lin, W. Cai, P. Huang, W. Tong, Y. Zou, Y. Xie, *Angew. Chem. Int. Ed.* **2015**, *54*, 11231-11235; *Angew. Chem.* **2015**, *127*, 11383-11387; d) S. Sun, G. Shen, J. Jiang, W. Mi, X. Liu, L. Pan, X. Zhang, J. Zou, *Adv. Energy Mater.* **2019**, *9*, 1901505.

[6] a) S. Sun, Y. Sun, Y. Zhou, S. Xi, X. Ren, B. Huang, H. Liao, L. P. Wang, Y. Du, Z. J. Xu, *Angew. Chem. Int. Ed.* **2019**, *58*, 6042-6047; *Angew. Chem.* **2019**, *131*, 6103-6108; b) C. Wei, Z. Feng, G. G. Scherer, J. Barber, Y. Shao-Horn, Z. J. Xu, *Adv. Mater.* **2017**, *29*, 1606800; c) Y. Zhou, S. Sun, J. Song, S. Xi, B. Chen, Y. Du, A. C. Fisher, F. Cheng, X. Wang, H. Zhang, Z. J. Xu *Adv. Mater.* **2018**, *30*, 1802912.

[7] J. B. Goodenough, P. M. Raccah, *J. Appl. Phys.* **1965**, *36*, 1031-1032.

[8] a) L. Wu, L. Sun, X. Li, Q. Zhang, H. Si, Y. Zhang, K. Wang, Y. Zhang, *Appl. Surf. Sci.* **2020**, *506*, 144964. b) D. Zhang, Y. Zhang, X. Li, Y. Luo, H. Huang, J. Wang, P. K. Chu, *J. Mater. Chem. A* **2016**, *4*, 568-577.

[9] Z. Liu, H. Cheng, N. Li, T. Ma, Y. Su *Adv. Mater.* **2016**, *28*, 3777-3784.

[10] C. Gong, X. Zhang, *Science* **2019**, *363*, 706.

[11] V. Gnezdilov, V. Fomin, A. V. Yeremenko, *Low Temp. Phys.* **2006**, *32*, 162-168.

[12] S. Sun, Y. Sun, Y. Zhou, J. Shen, D. Mandler, R. Neumann, Z. J. Xu, *Chem. Mater.* **2019**, *31*, 8106-8111.

[13] J. O. Bockris, T. Otagawa, *J. Electrochem. Soc.* **1984**, *131*, 290-302.

[14] a) W. Luo, X. Hu, Y. Sun, Y. Huang, *J. Mater. Chem* **2012**, *22*, 8916-8921; b) J. Brzeska, A. M. Elert, M. Morawska, W. Sikorska, M. Kowalczuk, M. Rutkowska, *Polymers* **2018**, *10*, 826; c) Y. Duan, S. Sun, S. Xi, X. Ren, Y. Zhou, G. Zhang, H. Yang, Y. Du, Z. J. Xu, *Chem. Mater.* **2017**, *29*, 10534-10541.

[15] a) K. Qiu, Y. Lu, D. Zhang, J. Cheng, H. Yan, J. Xu, X. Liu, J. K. Kim, Y. Luo, *Nano Energy* **2015**, *11*, 687-696; b) E. J. Crumlin, E. Mutoro, Z. Liu, M. E. Grass, M. D. Biegalski, Y. L. Lee, D. Morgan, H. M. Christen, H. Bluhm, Y. Shao-Horn, *Energy Environ. Sci.* **2012**, *5*, 6081-6088; c) D. Barreca, C. Massignan, S. Daolio, M. Fabrizio, C. Piccirillo, L. Armelao, E. Tondello, *Chem. Mater.* **2001**, *13*, 588-593; d) W. Wei, W. Chen, D. G. Ivey, *Chem. Mater.* **2008**, *20*, 1941-1947; e) S. Hao, B. Zhang, S. Ball, M. Copley, Z. J. Xu, M. Srinivasan, K. Zhou, S. Mhaisalkar, Y. Huang, *J. Power Sources* **2015**, *294*, 112-119.

[16] a) T. S. Herng, D. Qi, T. Berlijn, J. Yi, K. Yang, Y. Dai, Y. Feng, I. Santoso, C. Sánchez-Hanke, X. Gao, A. T. Wee, W. Ku, J. Ding, A. Rusydi, *Phys. Rev. Lett.* **2010**, *105*, 207201; b) X. Che, L. Li, G. Li, *Appl. Phys. Lett.* **2016**, *108*, 143102.

[17] S. Zhou, X. Miao, X. Zhao, C. Ma, Y. Qiu, Z. Hu, J. Zhao, L. Shi, J. Zeng, *Nature Commun.* **2016**, *7*, 11510.

[18] a) P. M. Raccah, J. B. Goodenough, *Phys. Rev.* **1967**, *155*, 932-943; b) M. A. Korotin, S. Y. Ezhov, I. V. Solovyev, V. I. Anisimov, D. I. Khomskii, G. A. Sawatzky, *Phys. Rev. B* **1996**, *54*, 5309-5316; c) C. Zobel, M. Kriener, D. Bruns, J. Baier, M. Grüninger, T. Lorenz, A. Revcolevschi, *Phys. Rev. B* **2002**, *66*, 020402.

[19] a) M. Karolak, M. Izquierdo, S. L. Molodtsov, A. I. Lichtenstein, *Phys. Rev. Lett.* **2015**, *115*, 046401; b) V. Křápek, P. Novák, J. Kuneš, D. Novoselov, Dm. M. Korotin, V. I. Anisimov, *Phys. Rev. B* **2012**, *86*, 195104; c) M. J. Hoch, S. Nellutla, J. Tol, E. S. Chol, J. Lu, H. Zheng, J. F. Mitchell, *Phys. Rev. B* **2009**, *79*, 214421.

[20] a) V. R. Galakhov, M. Demeter, S. Bartkowski, M. Neumann, N. A. Ovechkina, E. Z. Kurmaev, N. I. Lobachevskaya, Ya. M. Mukovskii, J. Mitchell, D. L. Ederer, *Phys. Rev. B* **2002**, *65*, 113102; b) L. Dahéron, R. Dedryvère, H. Martinez, M. Ménétrier, C. Denage, C. Delmas, D. Gonbeau, *Chem. Mater.* **2008**, *20*, 583-590.

[21] a) S. Sun, H. Li, Z. J. Xu, *Joule* **2018**, *2*, 1024-1027; b) C. Wei, R. R. Rao, J. Peng, B. Huang, I. E. Stephens, M. Risch, Z. J. Xu, Y. Shao-Horn, *Adv. Mater.* **2019**, *31*, 1806296; c) C. Wei, S. Sun, D. Mandler, X. Wang, S. Qiao, Z. J. Xu, *Chem. Soc. Rev.* **2019**, *48*, 2518-2534.

[22] L. Trotochaud, J. K. Ranney, K. N. Williams, S. W. Boettcher, *J. Am. Chem. Soc.* **2012**, *134*, 17253-17261.

[23] P. Gütlich, H. A. Goodwin, *Spin crossover—an overall perspective. Spin Crossover in Transition Metal Compounds I*, Springer, Berlin, Heidelberg, **2004**, pp. 1-47.

[24] T. A. Tyson, Q. Qian, C. C. Kao, J. P. Rueff, F. M. F. de Groot, M. Croft, S. W. Cheong, M. Greenblatt, M. A. Subramanian, *Phys. Rev. B* **1999**, *60*, 4665-4674.

COMMUNICATION

Engineering high-spin state cobalt cations in spinel $ZnCo_2O_4$ propagates a spin channel for spin-selected charge transport and enhances active sites for intermediate adsorption. High-spin cobalt cations can be directly engineered by varying the calcination temperature.

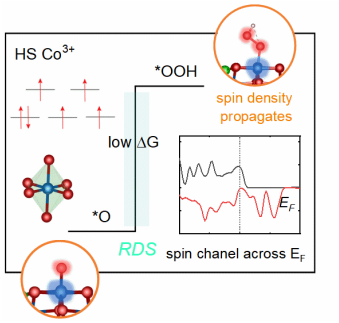

Yuanmiao Sun, Xiao Ren, Shengnan Sun, Zheng Liu, Shibo Xi, and Zhichuan J. Xu

Page No. – Page No.

Engineering High-Spin State Cobalt Cations in Spinel Zinc Cobalt Oxide for Spin Channel Propagation and Active Site Enhancement in Water Oxidation